Invited Paper

A large-area Sagnac interferometer using atoms in a time-orbiting potential

E. Moan[a], Z. Luo[a], and C. A. Sackett[a]

[a]Physics Department, University of Virginia, Charlottesville, VA, USA

ABSTRACT

We describe an implementation of a Sagnac interferometer using a Bose-Einstein condensate confined in a harmonic time-orbiting potential trap. Atoms are manipulated using Bragg laser beams to produce two reciprocal interferometers, providing common-mode rejection of accelerations, trap fluctuations, and most other effects. The Sagnac rotation phase is differential. The orbit of the atoms is nearly circular, with an effective Sagnac area of about 0.5 mm^2.

Keywords: Bose-Einstein condensate, atom interferometry, Sagnac interferometer

1. INTRODUCTION

Inertial navigation capabilities for vehicles play an important role in commercial travel, military systems, and space exploration. Sensitive and accurate rotation sensing is a critical requirement for such applications.[1] One effective technique used for rotation sensing is Sagnac interferometry, in which a wave is split, traverses two paths that enclose an area, and then recombined. The resulting interference signal depends on the rotation rate of the system and the area enclosed by the paths.[2] Indeed, optical Sagnac interferometers, in the form of fiber-optic gyroscopes, are an important component in present-day inertial navigation systems.[3] However, their limited sensitivity and tendency to drift are motivations to develop alternative techniques. Other applications for rotation sensing include north-finding,[4] geophysical analysis,[5] and tests of general relativity.[6]

Atom interferometry has long been suggested as a method to achieve better rotation sensing.[7] In this case, a Sagnac interferometer is implemented using quantum matter waves rather than light. Because a comparable de Broglie wavelength can be obtained at an atomic speed much lower than that of light, the interference phase is much more sensitive to rotation—by a factor of $mc^2/\hbar\omega$ for atom mass m, speed of light c, Planck's constant $\hbar$ and light frequency ω. This factor can be 10^{10} or larger, which explains the appeal of the atomic systems. However, atoms are much more difficult to manipulate than light, and atom interferometers created to date have had relatively small enclosed areas. Although atom interferometers have demonstrated superior gyroscope performance,[8,9] the benefits have not been large enough to offset the substantial increase in apparatus size and complexity that atomic systems require.

We report here on the implementation of an atomic Sagnac interferometer that may help overcome these problems. While most atom interferometers use atoms in free fall, ours is based on atoms confined in a magnetic trap. This allows the atoms to be supported against gravity so that a long measurement time can be achieved without requiring a large drop distance. The confining potential can also be used to control the trajectory of the atoms, causing them to move in a compact loop that provides the optimum enclosed area for a given travel distance and time. Finally, using trapped atoms may to be advantageous for practical inertial navigation applications because the trap can hold the atoms in place relative to an accelerating vehicle.

A few trapped-atom Sagnac interferometers have been demonstrated in the past.[10–13] The largest areas have been achieved using a linear interferometer (with no enclosed area) that is translated along a direction perpendicular to the interferometer axis.[14] We here demonstrate a true two-dimensional interferometer configuration in which atoms travel in circular trajectories through a static confining potential with an effective enclosed area

Further author information:
C.A.S.: E-mail: sackett@virginia.edu, Telephone: 1 434 924 6795

Optical, Opto-Atomic, and Entanglement-Enhanced Precision Metrology, edited by Selim M. Shahriar, Jacob Scheuer, Proc. of SPIE Vol. 10934, 109341X · © 2019 SPIE · CCC
code: 0277-786X/19/$18 · doi: 10.1117/12.2515457

2.5 times larger than previously observed. Our approach is readily scalable to weaker traps and multiple orbits by the atoms, making larger areas feasible.

A second key advance is the use of dual counter-propagating interferometer measurements. Here two Sagnac interferometers are implemented at the same time in the same trap, with atoms traveling at opposite velocities over the same paths. This technique was developed for free space interferometers,[8] and allows the common mode cancellation of interferometric phases from accelerations, laser noise, background fields, and other effects which can mask the rotation signal. The Sagnac effect itself is differential and can be extracted by comparing the two individual measurements. This technique is likely to be essential for any practical rotation-sensing system.

Using these techniques, we achieve a rotation sensitivity comparable to the Earth's rotation rate, 10^{-4} rad/s. A phase offset observed at zero rotation can be explained by residual sensitivity to the trap and laser beam alignment parameters, and we have identified methods to minimize this offset.

The remainder of this paper will explain the interferometer concept, describe the apparatus, present results, and discuss the outlook for further improvements.

2. INTERFEROMETER CONCEPT

The Sagnac interferometer is implemented using a Bose-Einstein condensate confined in a three-dimensional harmonic trap, with potential energy

$$V(x,y,z) = \frac{1}{2}m(\omega_x^2 x^2 + \omega_y^2 y^2 + \omega_z^2 z^2). \tag{1}$$

Here m is the atomic mass and the ω_i are the trapping frequencies. The coordinates x, y and z represent the principle axes of the trap. The trap is approximately cylindrically symmetric, with $\omega_x \approx \omega_y$. The condensate starts with an initial position $\mathbf{r}_0$ and initial velocity $\mathbf{v}_0$.

The condensate is manipulated using a set of standing wave Bragg lasers[15,16] propagating along the x' and y' directions. We allow the Bragg directions to vary from the trap principle axes, as

$$\hat{\mathbf{x}}' = \cos\theta_x \hat{\mathbf{x}} + \sin\theta_x \cos\phi_x \hat{\mathbf{y}} + \sin\theta_x \sin\phi_x \hat{\mathbf{z}} \tag{2}$$

and

$$\hat{\mathbf{y}}' = -\sin\theta_y \cos\phi_y \hat{\mathbf{x}} + \cos\theta_y \hat{\mathbf{y}} + \sin\theta_y \sin\phi_y \hat{\mathbf{z}}. \tag{3}$$

The Bragg beams couple atomic states with momenta $\mathbf{p}$ and $\mathbf{p} \pm 2\hbar\mathbf{k}$, where $\mathbf{k}$ is the wave vector of the laser beam. We express this in terms of velocity as $\mathbf{v} \leftrightarrow \mathbf{v} \pm v_B\hat{\mathbf{k}}$, where $v_B = 2\hbar k/m$ is the Bragg velocity imparted to the atoms.

In practice the initial condensate motion and Bragg beam misalignment must be taken into account, but to illustrate the operation of the the interferometer in a simple way, we assume for now the ideal case with $\mathbf{r}_0 = \mathbf{v}_0 = \theta_x = \theta_y = 0$ and $\omega_x = \omega_y = \omega$. We will return subsequently to the non-ideal case.

The interferometer measurement begins by applying the Bragg beams along $\hat{\mathbf{y}}$. This generates two wave packets moving with velocities $\mathbf{v} = \pm v_B\hat{\mathbf{y}}$. The atoms move in the trap, following the usual trajectory for a harmonic oscillator

$$x(t) = 0 \qquad y(t) = \pm\frac{v_B}{\omega}\sin\omega t. \tag{4}$$

The packets are allowed to move for time $t_1 \approx \pi/(2\omega)$, at which point the atoms have come to rest near the classical turning point at radius $R = v_B/\omega$. At this time, Bragg beams traveling along x are applied to both packets, providing velocity kicks $\pm v_B\hat{\mathbf{x}}$ and generating a total of four packets. Each of these packets now travels in a circle of radius R, as

$$x(t) = \pm R\sin\omega t \qquad y(t) = \pm R\cos\omega t. \tag{5}$$

The atoms are allowed to propagate for time $t_2 \approx 2\pi/\omega$, completing one full orbit around the trap. We assume that the density of the atoms is low enough that the packets can pass through each other with negligible interactions.

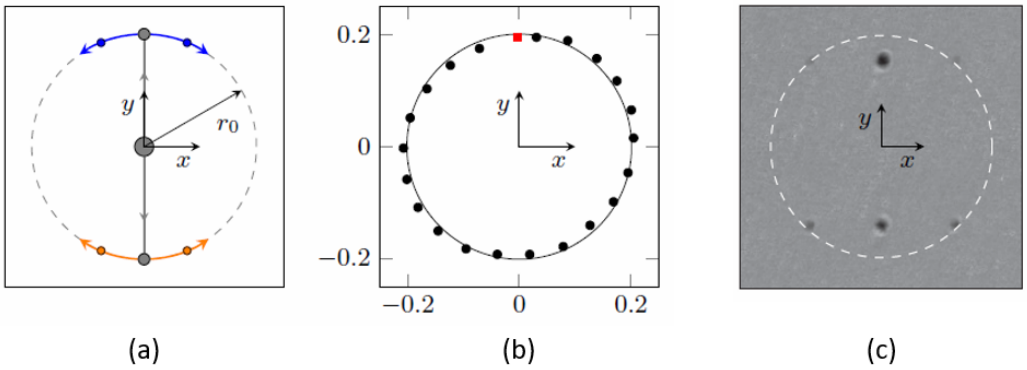

Figure 1. Trajectories of atoms in the interferometer. The images show the xy plane in which the atoms move. Part (a) shows a schematic of the motion, with different colors used to represent the trajectories of the different interferometers. Part (b) shows the measured positions of a single packet as it orbits around the trap, starting at the red square and moving clockwise. The scale is labeled in millimeters. Part (c) shows an absorption image of the interferometer output. The moving atoms continue their orbit on the dashed circle, while the atoms brought to rest have moved directly back towards the trap center.

After one orbit, the pairs of packets are overlapped again at their locations prior to the x Bragg pulse. The wave function of a pair can be expressed as

$$|\psi\rangle = \frac{1}{\sqrt{2}}\left(e^{i\Phi/2}|+v_B\rangle + e^{-i\Phi/2}|-v_B\rangle\right), \tag{6}$$

where Φ is the differential phase developed between the packets and $|\pm v_B\rangle$ are states with the indicated velocity along x. The x Bragg beams are now applied again. This couples the combination $(|+v_B\rangle + |-v_B\rangle)$ back to the zero-momentum state $|0\rangle$, while the asymmetric combination $(|+v_B\rangle - |-v_B\rangle)$ remains unchanged (up to an overall phase). Projecting the wave function $|\psi\rangle$ onto these combinations, we find that a fraction $N_0/N = \cos^2\Phi/2$ of the atoms are brought back to rest.[17,18] To detect the result of the recombination, the moving and stationary atoms are allowed to separate, and then the entire system is observed using absorption imaging. Note that this sequence produces two independent interference measurements. We define Φ_+ as the phase measured for atoms at $y = +R$, and Φ_- as the phase measured at $y = -R$.

Figure 1 shows a schematic of the atomic trajectories, measured positions of a packet as it traverses the trap, and typical results of an interference measurement.

The phase difference between two packets can be expressed as[19]

$$\Phi = \frac{1}{\hbar}\int_0^{t_2} (\mathcal{L}_1 - \mathcal{L}_2)\, dt + \Phi_L, \tag{7}$$

where $\mathcal{L}_i$ is the classical Lagrangian for packet i and Φ_L is the change in the Bragg laser phase between the initial and final x pulses. The Lagrangians can be integrated to give in the ideal case $\int \mathcal{L}\, dt = 0$. However, in a rotating frame, the Sagnac effect contributes an additional phase difference

$$\Phi_S = \frac{1}{\hbar}\oint \mathbf{L}\cdot\mathbf{\Omega}\, dt = \frac{2m\Omega A}{\hbar}, \tag{8}$$

where $\mathbf{L} = \mathbf{r}\times\mathbf{p}$ is the angular momentum, $\mathbf{\Omega}$ is the rotation vector of the frame and $A = 2\pi R^2$ is the total area enclosed by the trajectories. The Sagnac contribution is opposite for the two interferometers, leading to a phase difference

$$\Delta\Phi = \Phi_+ - \Phi_- = 2\Phi_S = \frac{8\pi m R^2\Omega}{\hbar}. \tag{9}$$

The laser phase Φ_L is the same for both packets, so it cancels in the difference and does not need to be controlled.

The interferometer output is more complicated in the non-ideal case, but can still be calculated analytically. The (non-rotating) Lagrangian separates as $\mathcal{L} = \mathcal{L}_x + \mathcal{L}_y + \mathcal{L}_z$ with

$$\mathcal{L}_s = \frac{m}{2}\left(v_s^2 + \omega_s^2 x_s^2\right), \tag{10}$$

and the motion for coordinate s is given by

$$x_s = x_{s0}\cos\omega_s t + \frac{v_{s0}}{\omega_s}\sin\omega_s t. \tag{11}$$

The motional phase acquired by a single packet over time t is then

$$\Phi_1 = \sum_s \frac{m}{4\hbar\omega_s}\Big[\left(v_{s0}^2 - \omega_s^2 x_{s0}^2\right)\sin 2\omega_s t - 2x_{s0}v_{s0}\omega_s\left(1-\cos\omega_s t\right)\Big], \tag{12}$$

and the net differential phase can be determined as

$$\Delta\Phi = 2\Phi_S + \frac{4mv_B^2}{\hbar}\sum_s \frac{\gamma_s}{\omega_s}\sin\omega_s t_2\,\cos\omega_s(t_1+t_2). \tag{13}$$

Here the γ_s are angular factors from the Bragg beams, with

$$\gamma_x = -\cos\theta_x\sin\theta_y\cos\phi_y \qquad \gamma_y = \cos\theta_y\sin\theta_x\cos\phi_x \qquad \gamma_z = \sin\theta_x\sin\theta_y\sin\phi_x\sin\phi_y. \tag{14}$$

We can Taylor expand the net phase around the ideal case, taking

$$\begin{aligned} \omega_x &= \omega(1+\Delta_\omega) & \omega_y &= \omega(1-\Delta_\omega) & \omega_z &= \kappa\omega \\ t_1 &= \frac{\pi}{2\omega}(1+\delta_1) & t_2 &= \frac{2\pi}{\omega}(1+\delta_2) & & \\ \theta_x - \theta_y &= \Delta_\theta & \theta_x + \theta_y &= 2\theta_t & & \end{aligned} \tag{15}$$

with dimensionless Δ_ω, δ_1, δ_2, and Δ_θ all assumed small compared to one. Although the misalignment Δ_θ between the Bragg beams is small, for a nearly symmetric trap the alignment of the principle axes is arbitrary and we cannot take θ_t small. We do not tune ω_z to any particular value, so κ is also large. We do introduce small parameters $\zeta_i = \sin\theta_i\sin\phi_i$ equal to the projection angle of Bragg beam i onto the z axis. Expanding around the small terms gives a leading-order behavior of

$$\begin{aligned} \Delta\Phi \approx 2\Phi_S &+ 8\pi^2 kR\left[\left(\delta_1 + 9\delta_2\right)\Delta_\omega\sin(2\theta_t) - \Delta_\theta\left(\delta_1\delta_2 + 4\delta_2^2 + 5\Delta_\omega^2\right)\right] \\ &+ \frac{8kR}{\kappa}\zeta_x\zeta_y\,\sin(2\pi\kappa)\,\cos(5\pi\kappa/2) \end{aligned} \tag{16}$$

Here the trap phase scaling is expressed using the Bragg laser wave number k and orbit radius R. For an effective rotation sensor, we require the trap phase terms in Eq. (16) to be small, or failing that, constant. Although $kR \sim 10^3$ is large, the error terms are each multiplied by at least two small factors.

3. APPARATUS

The interferometer is implemented using about 10^4 ^{87}Rb atoms in a trap with $\omega \approx 2\pi \times 9.3$ Hz and $\omega_z \approx 2\pi \times 12.4$ Hz. The apparatus for producing condensates and generating the magnetic trap is described in Ref. 20. Our time-orbiting potential (TOP) trap[21] uses a special field configuration that allows precise experimental control of the trap parameters. We focus here on how this control is implemented.

The bias field of the TOP trap rotates on the surface of a sphere in three dimensions, as

$$\mathbf{B}(t) = B_0\left[\left(1+\frac{\Delta_B}{2}\right)\cos\Omega_1 t\cos\left(\Omega_2 t + \frac{\beta}{2}\right)\hat{\mathbf{x}}' + \left(1-\frac{\Delta_B}{2}\right)\cos\Omega_1 t\sin\left(\Omega_2 t - \frac{\beta}{2}\right)\hat{\mathbf{y}}' + \sin\Omega_1 t\hat{\mathbf{z}}\right], \tag{17}$$

with $\Omega_1 \approx 2\pi \times 10^4$ Hz and $\Omega_2 \approx 2\pi \times 10^3$ Hz. Here Δ_B and β are small amplitude and phase imbalances. We obtain the desired cylindrical symmetry with $\Delta_B = \beta = 0$, but we include these terms to compensate for asymmetries arising from experimental imperfections. The coils producing the field are nominally aligned to the Bragg beam directions, so we express it in the primed coordinates. The trap also features an oscillating quadrupole field

$$\mathbf{B} = B_1 \left(\frac{x'}{2}\hat{\mathbf{x}}' + \frac{y'}{2}\hat{\mathbf{y}}' - z\hat{\mathbf{z}} \right) \sin \Omega_1 t. \tag{18}$$

The time-averaged potential produced by these fields is, to first order in Δ_B and β,

$$V = V_0 - \frac{1}{2}\mu B_1 z + \frac{1}{2}m\omega_z^2 z^2 + \frac{1}{2}m\omega^2 \left[\left(1 + \frac{\Delta_B}{7} \right) x'^2 + \left(1 - \frac{\Delta_B}{7} \right) y'^2 + \frac{2}{7}\beta x' y' \right], \tag{19}$$

with

$$\omega^2 = \frac{7}{64}\frac{\mu B_1^2}{mB_0} \qquad \omega_z^2 = \frac{1}{8}\frac{\mu B_1^2}{mB_0} \tag{20}$$

for atoms with magnetic moment μ. We use atoms in the $F = 2, m_F = 2$ state where μ is equal to the Bohr magneton μ_B. We set $B_1 = 2mg/\mu_B \approx 31$ G/cm so that the linear term cancels gravity and provides a potential minimum at $\mathbf{r} = 0$. In practice, the bias field is not perfectly uniform and itself has a non-zero curvature. This shifts the trap frequencies relative to (20), but the dependence on Δ_B and β in Eq. (19) remains.

The trap principle coordinates (x, y) are determined by diagonalizing the quadratic form in (19). This gives trap frequencies

$$\omega_{x,y}^2 = \omega^2 \left(1 \pm \frac{1}{7}\sqrt{\Delta_B^2 + \beta^2} \right), \tag{21}$$

and the angle θ_t between the Bragg and trap axes is determined by

$$\tan \theta_t = \frac{\beta}{\sqrt{\Delta_B^2 + \beta^2} - \Delta_B}. \tag{22}$$

This is the angle appearing in Eq. (16), so we see how θ_t and Δ_ω can be controlled in the experiment. With a little further analysis, we obtain

$$\Delta_\omega = \frac{1}{14}\sqrt{\Delta_B^2 + \beta^2} \tag{23}$$

and

$$\Delta_\omega \sin 2\theta_t = \frac{1}{14}\beta. \tag{24}$$

The x Bragg beam can be finely adjusted using a translation stage and mirror mount, achieving approximately 5×10^{-4} rad resolution in θ_x and ϕ_x. The y Bragg beam travels through a thin vacuum tube before reaching the atoms, so it is more difficult to adjust.

The atoms can be imaged both vertically, showing the xy plane as in Fig. 1(c), and horizontally, showing the xz plane. Since the direction of a Bragg beam can be determined by observing the velocity kicks it produces, we can use the images to initially align the beams and ensure that the relative alignment error Δ_θ is small. Similarly, the trap can be made approximately symmetric by observing the oscillation period of atoms after receiving a single Bragg kick. Finer adjustments are then made by measuring the trajectories of the atoms in the interferometer and ensuring that both pairs of packets overlap after completing one orbit.

4. RESULTS

When the Bragg beam and trap parameters are adjusted correctly, we observe simultaneous interference for both packet pairs. Each individual interferometer exhibits phase noise, primarily due to vibrations of the mirror used to retro-reflect the x Bragg beam. The appearance of this noise is an indicator that inference is occurring. Figure 2 shows the standard deviation of the the interferometer signals $S = N_0/N$ as the trajectory time t_2 is varied. It can be seen that the interferometers operate at the same time. The usable range Δt_2 of time values

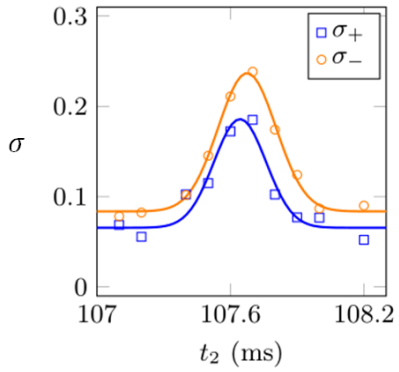

Figure 2. Simultaneous interference of the two interferometers. Blue squares show the standard deviation of the interference signal for the interferometer at $y = +R$, and orange circles show the standard deviation for the interferometer at $y = -R$. Both are plotted as functions of the time t_2 at which the recombination pulse is applied. Solid curves are Gaussian fits to guide the eye.

is determined by the size ℓ of the condensates, since the wave packets must overlap in space. The observed condensate size is approximately 10 μm, consistent with the Thomas-Fermi approximation for our trap.[22] The predicted overlap time $\ell/2v_B \approx 0.5$ ms agrees well with the observed Δt_2. The baseline value of σ away from the peak indicates the level of imaging noise. The amplitudes of the peaks are consistent with an interferometer visibility of about 0.5.

When the two signals S_+ and S_- are plotted against each other, the data fall on an elliptical curve.[23] To understand this, assume that the signals can be described by

$$S_\pm = C_\pm + A_\pm \sin\left(\Phi_L \pm \frac{\Delta\Phi}{2}\right), \tag{25}$$

where $C_\pm$ are the signal centers and $A_\pm$ the interference amplitudes. Here Φ_L incorporates all common-mode phases, and will fluctuate from shot to shot. If we define $X = (S_+ - C_+)/A_+ = \sin(\Phi_L + \Delta\Phi/2)$ and $Y = (S_- - C_-)/A_- = \sin(\Phi_L - \Delta\Phi/2)$, we immediately find

$$\frac{1}{2}\left(X^2 + Y^2\right) = \sin^2\Phi_L \cos^2(\Delta\Phi/2) + \cos^2\Phi_L \sin^2(\Delta\Phi/2) \tag{26}$$

and

$$XY = \sin^2\Phi_L \cos^2(\Delta\Phi/2) - \cos^2\Phi_L \sin^2(\Delta\Phi/2). \tag{27}$$

The fluctuating term Φ_L can then be eliminated using $\sin^2\Phi_L + \cos^2\Phi_L = 1$, leading to the equation for an ellipse:

$$X^2 + Y^2 - 2XY\cos\Delta\Phi = \sin^2\Delta\Phi. \tag{28}$$

We observe ellipses of this form, as seen in Fig. 3(a). By fitting to the ellipse, we extract the centers $C_\pm$, amplitudes $A_\pm$, and phase $\Delta\Phi$. The data shown provide an accuracy in $\Delta\Phi$ of 0.2 rad, about fifty times larger than the shot-noise limit here.

Ideally, the differential phase should be equal to $2\Phi_S$, which is about 0.1 rad for Earth rotation at the latitude of Charlottesville, VA. The measured results deviate from this value, which we attribute to the trap phase contributions of Eq. (16). For instance, Fig. 3(a) shows that $\Delta\Phi$ depends on the interferometer time t_2, corresponding to the shift δ_2 in (16). As seen in part (b), the dependence on t_2 is linear with a slope $d\Delta\Phi/dt_2$ of about 5 rad/ms. As predicted, the slope itself varies linearly with the trap phase parameter β, with an observed second derivative $d^2\Delta\Phi/dt_2 d\beta \approx 4 \times 10^5$ s^{-1}.

This measured dependence is about a factor of two smaller than predicted by Eq. (16). The reason for this has not be identified, but we expect it can be attributed to inaccuracy of our trap model. As noted, curvatures

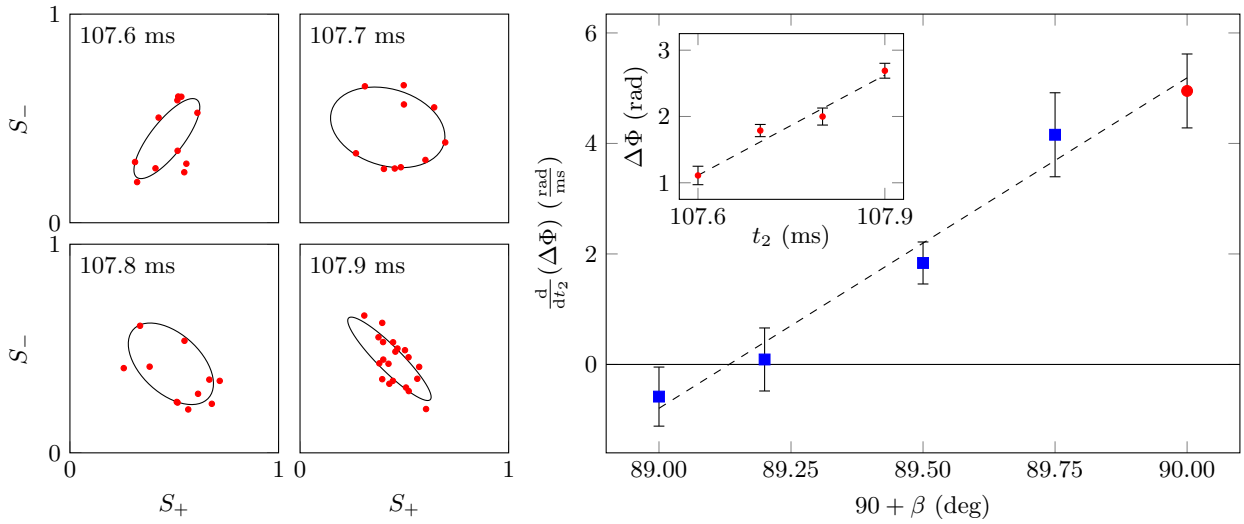

Figure 3. Interferometer measurements. (a) Each red points is an individual pair of (S_+, S_-) results obtained from a run of the interferometer. As the common-mode phase fluctuates, the points fall on an ellipse. Curves show the best fit ellipses. The four plots are taken at different measurement times t_2. The differential phases then vary from X to Y. (b) The inset shows the four results from part (a), plotted against t_2. The main plot shows the slope $(d/dt_2)\Delta\Phi$ as a function of the trap phase parameter β. The red point corresponds to the inset data.

of the bias field cause the trap frequencies to differ from the simple result of Eq. (20). This could change the dependence of the trap frequencies on β. Alternatively, anharmonic terms in the potential may also contribute to the observed phase. While the explanation for this discrepancy will need to be determined, data such as in Fig. 3 illustrates that the interferometer functions reliably with an inferred rotation sensitivity close to Earth rate.

5. OUTLOOK

As this is the first demonstration of this type of interferometer, many improvements can be readily envisioned. The data of Fig. 3 show already how we can use the dependence of the signal on trap parameters to locate a configuration where the unwanted trap phase contribution is zero. Here we can identify a value of β where the measured phase becomes independent of t_2 to first order, indicating that the true value of β in the experimental trap potential is zero. It is similarly possible to tune δ_1 and δ_2 to make the phase independent of β, and by operating at the optimum conditions for both, the horizontal trap phase terms in (16) will be well suppressed. The z trap phase term can be suppressed in a similar way by adjusting the Bragg beam orientations. By these methods, we hope to isolate the Sagnac terms and achieve absolute rotation sensitivity.

At present, the cycle time of the experiment is limited to one run every few minutes, in part because our evaporative cooling process is slow but also because running more rapidly causes the trap to heat up and the interferometer to become unstable. We are planning to upgrade to a system using an atom chip to generate the trap,[24] which will provide both faster evaporation and better heat sinking of the trap coil elements.[25] We can also explore the use of phase-contrast techniques to reduce imaging noise.[26]

The rotation sensitivity itself can be increased in several ways. If the trap frequency ω is reduced, the atoms will move in a larger radius orbit R and enclose a bigger area. Since the Sagnac phase scales as R^2 while the trap phase in (16) scales as R, this should be advantageous. Alternatively, we could use a higher-order Bragg process to increase v_B.[27] This also increases R, but avoids lengthening the interferometer measurement time. Finally, it should be possible to let the atoms make multiple orbits around the trap before completing the interferometer. This again increases the effective Sagnac area. It seems plausible to achieve ten orbits in a trap with $R = 1$ mm, which would yield a shot-noise limited rotation sensitivity of 10^{-8} (rad/s)/$\sqrt{\text{Hz}}$. This is about 10^5 times larger

than the initial performance observed here, but of that a factor of 400 comes from improvements to condensate production and imaging which rely only on previously demonstrated techniques.

Anharmonicity of the trap potential is likely to become an important factor as performance improves. Numerical modeling suggest that the Sagnac signal is particularly sensitive to $\rho^2 z$ and ρ^4 terms, with $\rho^2 = x^2 + y^2$. These terms can be controlled by careful design of the magnetic coils used to generate the trap, but they can also be manipulated in the TOP trap by using fields with more complicated time dependence than in Eq. (17).

In summary, we have demonstrated the first trapped-atom Sagnac sensor using dual counter-rotating interferometers to obtain common-mode noise rejection. We achieve rotation sensitivity close to Earth rate, and the phase dependence on the trap parameters agrees reasonably well with a simple model. We hope to develop this approach into a useful technique for precise rotation sensing.

ACKNOWLEDGMENTS

Adam Fallon, Seth Berl, Tanwa Arpornthip and Robert Horne have all made contributions to this work. The present effort is funded by NASA under contract number 1502012, with previous funding from the NSF and the DARPA gBECi program.

REFERENCES

[1] Titterton, D. and Weston, J. L., [*The RF and Microwave Handbook*], Institution of Engineering and Technology, London, 2nd ed. (2004).

[2] Sagnac, G., "L'éther lumineux démontré par l'éffet du vent relatif d'éther dans un interférometre en Allan variance analysis rotation uniforme," *C. R. Acad. Sci.* **95**, 708 (1913).

[3] Lefère, H. C., [*The Fiber-Optic Gyroscope*], Artech House, Norwood, MA, 2nd ed. (2014).

[4] Prikhodko, I. P., Zotov, S. A., Trusov, A. A., and Shkel, A. M., "What is MEMS gyrocompassing? Comparative analysis of maytagging and carouseling," *J. Microelectromech. Syst.* **22**, 1257 (2013).

[5] Stedman, G. E., "Ring-laser tests of fundamental physics and geophysics," *Rep. Prog. Phys.* **60**, 615 (1997).

[6] Cerdonio, M., Prodi, G. A., and Vitale, S., "Dragging of inertial frames by the rotating earth—proposal and feasibility for a ground-based detection," *Gen. Rel. Grav.* **13**, 185 (1988).

[7] Gustavson, T. L., Landragin, A., and Kasevich, M. A., "Rotation sensing with a dual atom-interferometer Sagnac gyroscope," *Class. Quantum Grav.* **17**, 2385 (2000).

[8] Durfee, D. S., Shaham, Y. K., and Kasevich, M. A., "Long-term stability of an area-reversible atom-interferometer Sagnac gyrosope," *Phys. Rev. Lett.* **97**, 240801 (2006).

[9] Savoie, D., Altorio, M., Fang, B., Sidorenkov, L. A., Geiger, R., and Landragin, A., "Interleaved atom interferometry for high-sensitivity inertial measurements," *Sci. Adv.* **4**, eaau7948 (2018).

[10] Jo, G.-B., Shin, Y., Will, S., Pasquini, T. A., Saba, M., Ketterle, W., Pritchard, D. E., Vengalattore, M., and Prentiss, M., "Long phase coherence time and number squeezing of two Bose-Einstein condensates on an atom chip," *Phys. Rev. Lett.* **98**, 030407 (2007).

[11] Wu, S., Su, E., and Prentiss, M., "Demonstration of an area-enclosing guided-ataom interferomter for rotation sensing," *Phys. Rev. Lett.* **99**, 173201 (2007).

[12] Burke, J. H. T. and Sackett, C. A., "A scalable Bose-Einstein condensate Sagnac interferometer in a linear trap," *Phys. Rev. A* **80**, 061603(R) (2009).

[13] Qi, L., Zhaohui, H., Valenzuela, T., Zhang, Y., Zhai, Y., Quan, W., Waltham, N., and Fang, J., "Magnetically guided Cesium interferometer for inertial sensing," *App. Phys. Lett.* **110**, 153502 (2017).

[14] Wu, S., Rooijakkers, W., Striehl, P., and Prentiss, M., "Bidirectional propagation of cold atoms in a 'stadium'-shaped magnetic guide," *Phys. Rev. A* **70**, 013409 (2004).

[15] Giltner, D. M., McGowan, R. W., and Lee, S. A., "Theoretical and experimental study of the Bragg scattering of atoms from a standing light wave," *Phys. Rev. A* **52**, 3966–3972 (1995).

[16] Hughes, K. J., Deissler, B., Burke, J. H. T., and Sackett, C. A., "High-fidelity manipulation of a Bose-Einstein condensate using an optical standing wave," *Phys. Rev. A* **76**, 035601 (2007).

[17] Wang, Y. J., Anderson, D. Z., Bright, V. M., Cornell, E. A., Diot, Q., Kishimoto, T., Prentiss, M., Saravanan, R. A., Segal, S. R., and Wu, S., "Atom Michelson interferometer on a chip using a Bose-Einstein condensate," *Phys. Rev. Lett.* **94**, 090405 (2005).

[18] Garcia, O., Deissler, B., Hughes, K. J., Reeves, J. M., and Sackett, C. A., "Bose-Einstein-condensate interferometer with macroscopic arm separation," *Phys. Rev. A* **74**, 031601(R) (2006).

[19] Berman, P. R., ed., [*Atom Interferometry*], Academic Press, San Diego (1997).

[20] Horne, R. A. and Sackett, C. A., "A cylindrically symmetric magnetic trap for compact Bose-Einstein condensate atom interferometer gyroscopes," *Rev. Sci. Instrum.* **88**, 013102 (2017).

[21] Petrich, W., Anderson, M. H., Ensher, J. R., and Cornell, E. A., "Stable, tightly confining magnetic trap for evaporative cooling of neutral atoms," *Phys. Rev. Lett.* **74**, 3352 (1995).

[22] Dalfovo, F., Giorgini, S., Pitaevskii, L., and Stringari, S., "Theory of Bose-Einstein condensation in trapped gases," *Rev. Mod. Phys.* **71**, 463 (1999).

[23] Foster, G. T., Fixler, J. B., McGuirk, J. M., and Kasevich, M. A., "Method of phase extraction between coupled atom interferometers using ellipse-specific fitting," *Opt. Lett.* **27**, 951 (2002).

[24] Reichel, J., "Microchip traps and Bose-Einstein condensation," *Appl. Phys. B* **74**, 469 (2002).

[25] Farkas, D. M., Hudek, K. M., Salim, E. A., Segal, S. R., Squires, M. B., and Anderson, D. Z., "A compact, transportable, microchip-based system for high repetition rate production of Bose-Einstein condensates," *App. Phys. Lett.* **96**, 093102 (2010).

[26] Gross, C., Zibold, T., Nicklas, E., Estève, J., and Oberthaler, M. K., "Nonlinear atom interferometer surpasses classical precision limit," *Nature* **464**, 1165 (2010).

[27] Müller, H., Chiow, S. W., Long, Q., Herrmann, S., and Chu, S., "Atom interferometry with up to 24-photon-momentum-transfer beam splitters," *Phys. Rev. Lett.* **100**, 180405 (2008).